A&A 371, 186–197 (2001)
DOI: 10.1051/0004-6361:20010334

Astronomy & Astrophysics

A reconsideration of disk properties in Herbig Ae stars⋆

A. Natta[1], T. Prusti[2], R. Neri[3], D. Wooden[4], V. P. Grinin[5,6],, and V. Mannings[7]

[1] Osservatorio Astrofisico di Arcetri, Largo E. Fermi 5, 50125 Firenze, Italy
[2] Astrophysics Division, Space Science Department of ESA, ESTEC, PO Box 299, 2200 AG Noordwijk, The Netherlands
[3] IRAM, 300 rue de la Piscine, Domaine Universitaire, 38406 St. Martin d'Hères Cedex, France
[4] NASA-Ames Research Center, Moffett Field, CA 94035, USA
[5] Crimean Astrophysical Observatory, Crimea, 334413 Nauchny, Ukraine
[6] St. Petersburgh University, 198904 St. Petersburgh, Russia
[7] SIRTF Science Center, California Institute of Technology, MS 314-6, Pasadena, CA 91125, USA

Received 12 February 2001 / Accepted 5 March 2001

Abstract. This paper presents state-of-the-art spectral energy distributions (SEDs) of four Herbig Ae stars, based in part on new data in the mid and far-infrared and at millimeter wavelengths. The SEDs are discussed in the context of circumstellar disk models. We show that models of irradiated disks provide a good fit to the observations over the whole range of wavelengths. We offer a possible solution to the long-standing puzzle caused by the excess emission of Herbig Ae stars, where a large fraction of the stellar luminosity is re-radiated between ∼1.25 and 7 μm, with a peak at about 3 μm. We suggest that this general behaviour can be caused by dust evaporation in disks where the gas component is optically thin to the stellar radiation, as expected if the accretion rate is very low. The creation of a puffed-up inner wall of optically thick dust at the dust sublimation radius can account for the near-infrared characteristics of the SEDs. It can also naturally explain the H and K band interferometric observations of AB Aur (Millan-Gabet et al. 2001), which reveal a ring of emission of radius ∼0.3 AU. Finally, irradiated disk models can easily explain the observed intensity of the 10 μm silicate features and their variation from star to star.

Key words. circumstellar matter – stars: formation

1. Introduction

The environment of Herbig Ae/Be stars (HAeBe) has been a source of debate for many years (see, for example, Waters & Waelkens 1998). It is clear, today, that there are large differences between the most massive stars in this group (corresponding to spectral types B5-B0; HBe in the following), and the less massive ones, that will be called for simplicity in the following HAe stars (Natta et al. 2000a). In HAe stars, we have strong evidence of the presence of circumstellar disks from millimeter interferometry (Mannings & Sargent 1997, 2000) and from direct images in the visual (Grady et al. 1999, 2000). This is not the case for HBe stars. However, even for HAe stars there is great uncertainty on the structure of the disks, with arguments for the existence of a roughly spherically distributed dust component (Di Francesco et al. 1994). As a consequence, the spectral energy distributions (SED) of HAe stars have been interpreted as the emission of extended spherical envelopes of low optical depth (Pezzuto et al. 1997; Miroshnichenko et al. 1997; Il'in & Krivova 2000), of circumstellar disks (Hillenbrand et al. 1995; Chiang et al. 2001), or of a combination of both (Natta et al. 1993; Miroshnichenko et al. 1999). Given the number of free parameters and the fact that the SED is not uniquely defined, all the fits are equally good (or equally bad).

The major difficulty in reproducing the SEDs of HAe stars with disk models is their inability to account at the same time for the shape and for the luminosity of the near-infrared excess, as discussed by Hartmann et al. (1993). These authors have pointed out that the high accretion rates required by the large near-infrared luminosities (Hillenbrand et al. 1995) are not consistent with the lack of emission from hot material (dust or gas) which results in the typical "3 μm bump" shape of the HAe SEDs. They suggested that the near-infrared emission could be

Send offprint requests to: A. Natta,
e-mail: natta@arcetri.astro.it

⋆ Based in part on observations obtained with ISO and with the IRAM Plateau de Bure Interferometer. ISO is an ESA project with instruments funded by ESA Member States (especially the PI countries: France, Germany, The Netherlands and the UK) and with the participation of ISAS and NASA. IRAM is supported by INSU/CNRS (France), MPG (Germany) and IGN (Spain).

due to transiently heated grains and PAHs in the immediate surroundings of the stars. This, however, was not confirmed by theoretical models (Natta & Krügel 1995) nor by ISO spectra of HAe stars (van den Ancker 1999).

The aim of this paper is to rediscuss the disk hypothesis in HAe stars taking advantage of the new and much improved SEDs that have recently become available over a large range of wavelengths. We have selected a small sample of four stars, which includes three highly variable stars, belonging to the subgroup of so-called UX Ori-type HAe stars or UXORs (UX Ori, WW Vul and CQ Tau) and one HAe star with much smaller photometric variability (AB Aur). The properties of UXORs have been summarized in a number of papers (see, for example, Grinin 1994). Most of them can be accounted for by models where a flared, optically thick circumstellar disk seen almost edge-on surrounds the star (Natta & Whitney 2000). Occasionally, the star is occulted by a dust condensation along the line of sight, of unknown origin, which causes deep photometric minima in the visual. It is likely that strong variability is seen only under favorable orientation with respect to the observer.

Our sample was chosen to allow a discussion of the SED in terms of circumstellar disks in objects where the existence and some of the disk properties are independently known. Secondly, we hoped to investigate further the evolutionary stage of UXORs and to shed some light on the location of the dust inhomogeneities that cause the photometric variability of the stars.

The plan of the paper is as follows. In Sect. 2 we describe new interferometric observations of WW Vul, as well as unpublished ISO data for WW Vul and CQ Tau and new ground-based 10 μm spectra of CQ Tau and UX Ori. In Sect. 3 we present the results of these new observations and the SEDs of the four stars. Section 4 is dedicated to a detailed comparison of the SEDs with the predictions of disk models. In Sect. 5 we discuss some of the implications of the proposed disk structure and summarize our conclusions.

2. Observations

2.1. Basic stellar properties

Table 1 reports the properties of the four stars. Column 1 gives the name of the star, Col. 2 the distance and Col. 3 the spectral type (see van den Ancker et al. 1999a; Rostopchina 1999 and references therein). Effective temperature (Col. 4), luminosity (Col. 5) and extinction (Col. 6) have been recomputed by us using the available photometry and standard methods. Column 7 shows for each star the maximum observed variability ΔV. UX Ori, WW Vul and CQ Tau show large photometric variability and deep minima, associated with a large increase in the polarization (Grinin 1994 and references therein). AB Aur is photometrically much more stable , with variations of small amplitude ($\Delta V \sim 0.25$ mag; Herbst & Shevchenko 1999). However, there is a report in the literature of a minimum of about 1 mag in 1997 (Kawabata et al. 1998; Ashok et al. 1999; van den Ancker et al. 1999b). It is possible that the rarity of deep photometric minima in AB Aur is due to the fact that we see its disk close to face-on (see following).

Column 8 shows the inclination of the disk with respect to the observer ($\theta = 90^\circ$ for an edge-on disk). For WW Vul, UX Ori and CQ Tau, the inclination is inferred from the degree of polarization at minimum light (Natta & Whitney 2000). For AB Aur, Grady et al. (1999) estimate $\theta < 45^\circ$ from an HST image in scattered light, while Mannings & Sargent (1997) derive $\theta \sim 76^\circ$ from the elongation of the ^{13}CO (1–0) emission. The small inclination derived by Grady et al. is confirmed by recent interferometric observations at Plateau de Bure (Dutrey et al., private communication) and we will adopt in the following $\theta = 30^\circ$.

2.2. Millimeter interferometry

Observations of WW Vul were made simultaneously at 2.9 mm and 1.2 mm using the Plateau de Bure interferometer (IRAM, Plateau de Bure – France) on October 31 and November 15, 1999. Visibilities were obtained in the most compact configuration of the 5 antenna array, yielding projected baselines which range from about 64 m down to the antenna diameter of 15 m. The 46″ (20″ at 1.2 mm) primary beam field of the interferometer was centered at $\alpha_{\rm J2000}$ =19:25:58.75 and $\delta_{\rm J2000}$ = +21:12:31.3.

At 1.2 mm, data were taken in double sideband mode with the receivers tuned to 240.0 GHz (upper sideband). At 2.9 mm, observations were made in upper sideband only, with the SIS receivers tuned to 105.0 GHz. The spectral correlators covered an effective bandwidth of 420 MHz, equivalent to a velocity range of 520 km s^{-1} at 1.2 mm (1200 km s^{-1} at 2.9 mm).

Visibilities were obtained using on-source integration times of 20 min interspersed with 4 min calibration on 1923+210. The atmospheric phase noise on the most extended baselines ranged between 7° and 15° at 2.9 mm (17° and 34° at 1.2 mm), consistent with seeing conditions (0.9″–1.0″) typical for late-fall weather conditions. The absolute flux density scale which was established on the basis of cross-correlations on the continuum of the radio star MWC 349 (1.06 Jy at 2.9 mm, 1.75 Jy at 1.2 mm), is in full agreement with the interferometric efficiency and should be accurate to 5% at 2.9 mm and to about 15% at 1.2 mm. The receiver passband shape was determined on 3C 454.3 and was measured better than 5% throughout the observations.

Data calibration was performed in the antenna-based manner. Flux densities of WW Vul were obtained from the visibilities using standard IRAM fitting procedures. At 1.2 mm, we derived a one σ continuum point source sensitivity limit of 1.1 mJy/beam corresponding to a rms brightness temperature of 3.1 mK, fully consistent with a total on-source integration time of 400 min and a mean

system temperature of 350 K. At 2.9 mm, we obtained a continuum sensitivity limit of 0.3 mJy/beam, roughly equivalent to a rms brightness temperature of 1 mK.

A continuum source was detected at 1.2 mm and 2.9 mm almost at the position of the array's phase tracking center. The source was well-detected on all baselines and must be smaller than 0.9″. The source is likely to be point-like, the gaussian model fitted to the visibility profile at 1.2 mm being fully consistent with the signal-to-noise level, and the mean atmospheric seeing conditions.

2.3. ISO

The ISOPHOT observations of WW Vul were obtained April 12, 1997. The photometric measurements of WW Vul were part of an ISO programme aimed at studying the circumstellar environment of UXORs. The sequence contained a spectrophotometric measurement (TDT = 51300108, observing mode PHT40), a background photometric measurement two arc minutes off target (51300109, PHT03), a photometric measurement (51300110, PHT03) and small maps at 150 and 200 μm (51300106, PHT22). The spectrophotometric measurement was done with 256 s integration time in the wavelength ranges 2.5–4.8 and 5.8–11.6 μm with resolving power of about 90. The off measurement was done with 32 s integration time per filter at 3.6, 7.3, 12, 25, 60 and 100 μm. The apertures were 18″ for the three shortest wavelengths, 52″ for 25 μm and 120″ for the two longest wavelengths. The on-target photometric measurement was done with the same filter, aperture and integration time set-up. The 150 and 200 μm maps were made with the array in spacecraft raster mode with steps of one pixel. This resulted in images with 92″ pixels at 150 and 200 μm. The on-target pointings were centred on $\alpha_{\rm J2000}$ = 19:25:58.6 and $\delta_{\rm J2000}$ = 21:12:31 while the background measurement was at $\alpha_{\rm J2000}$ = 19:25:58.6 and $\delta_{\rm J2000}$ = 21:14:31.

The data were reduced with PIA (Gabriel et al. 1997). In the reductions, we followed the standard off-line processing steps with the following exceptions. For the 3.6–100 μm photometry we sub-divided the ramps into 8 parts in order to allow a better treatment of measurements where the response was drifting during the integration. For the spectrophotometry, we used also so-called dynamic calibration where every wavelength is calibrated individually against a standard star which has its flux at the corresponding wavelength close to that of WW Vul. In all cases, the statistical errors are much less than the quoted calibration accuracies of 10–20%.

The 150 and 200 μm maps do not show any clear detection of a point source. This is due to the fact that the background fluctuation is at least as strong as the flux of WW Vul at these wavelengths. Therefore, we could not extract flux values from these measurements.

The LWS observation of CQ Tau was obtained February 15, 1998 (82301814, LWS01). The observation covered the full LWS wavelength range from 43 to 196 μm.

Table 1. Stellar properties

(1)	(2)	(3)	(4)	(5)	(6)	(7)	(8)
Star	D (pc)	ST	$T_\star$ (K)	$L_\star$ ($L_\odot$)	A_V (mag)	ΔV (mag)	θ (deg)
AB Aur	140	A0	9500	48	0.5	0.25	<45
CQ Tau	100	F2	7500	5	0.9	2.1	66
UX Ori	450	A3	8600	42	0.4	2.2	60
WW Vul	550	A3	8600	43	0.6	1.9	53

We used the automatically processed data after omitting detector SW1 which is known to have occasionally strange behaviour and which in the case of CQ Tau deviated from the other measurements.

2.4. 10 micron spectrophotometry

Multi-epoch 10 μm spectrophotometry was obtained for CQ Tau on 5 November 1997 UT, 6 November 1997 UT, and 25 September 1998 UT using the Hi-Efficiency Faint Object Grating Spectrometer (HIFOGS, Witteborn et al. 1995) at the Wyoming Infrared Observatory (WIRO) using conventional infrared observing techniques. The HIFOGS spectral range spans the 7.5−13.4 μm atmospheric window with 120 discrete Bi:Si detectors at an approximately constant resolution of $\Delta\lambda$ = 0.05 μm per detector. HIFOGS used a 3″ circular aperture and a 30″ chop throw. The spectra of CQ Tau were flux calibrated with the bright IR standard star α Tau, using the well determined flux spectrum by Cohen et al. (1996). Differences in atmospheric transmission between CQ Tau and α Tau spectra were corrected using the ratio of telluric transmissions calculated by ATRAN (Lord 1993) for a total column of 4.5 mm of H_2O for WIRO. The method of telluric correction was confirmed by dividing the same standard star taken at several different air masses by its measurement at the lowest air mass; applying telluric corrections to these ratios yielded 1.00 ± 0.02 for the photometric nights 6 Nov. 97 UT and 25 Sep. 98 UT. Standard star measurements on 5 Nov. 97 UT showed large photometric uncertainties of up to 12%, and telluric corrections good to 2%–5% in the shape of H_2O (7.5−7.8 μm), O_3 (9.4−9.8 μm), and CO_2 (13.0−13.4 μm) bands. The three nights of 10 μm spectra of CQ Tau that were obtained showed no significant variations in either spectral shape or flux level of the silicate resonance and mid-IR continuum to a level of the photometric accuracy of the observations. From the three night spectra of CQ Tau, a single statistically-weighted average spectrum was calculated with a resulting signal-to-noise greater than 20.

Multi-epoch HIFOGS 10 μm spectrophotometry was also obtained for UX Ori on two observing runs at WIRO in October 1996 and November 1997. The photometric stability of the sky was not as good for UX Ori as for CQ Tau. The sky conditions during the October 1996 HIFOGS observing run were consistently better than during the November 1997. One night, 11 October 1996 UT

Table 2. Millimeter interferometry

(1)	(2)	(3)	(4)	(5)	(6)	(7)	(8)	(9)	(10)	(11)	(12)
Star	Position (J2000)		λ_1	S	λ_2	S	$\alpha_{\rm mm}$	$FWHM$	Mass	Telescope	Ref.
	α	δ	(mm)	(mJy)	(mm)	(mJy)		($''$)	($M_\odot$)		
AB Aur	04:52:34.3	+30:28:20.1	–	–	2.7	10.6 ± 0.4	$3.1 \pm 0.3^\dagger$	$<2^{\dagger\dagger}$	0.02	OVRO	a
CQ Tau	05:32:54.13	+24:43:03.9	1.2	151 ± 3	3.4	13.0 ± 1	2.6 ± 0.1	1.0	0.03	PdB	b
UX Ori	05:04:30.00	−03:47:14.3	1.2	19.8 ± 2.0	2.6	3.8 ± 0.4	2.1 ± 0.2	<0.5	0.05	PdB	c
WW Vul	19:25:58.74	+21:12:31.3	1.2	9.1 ± 1	2.9	1.2 ± 0.3	2.3 ± 0.4	<0.9	0.05	PdB	d

† There are no 1.3 mm interferometric observations of AB Aur. $\alpha_{\rm mm}$ is computed using the single-dish flux 103 ± 18 (Mannings 1994). †† from 2.6 mm OVRO observations. References: (a) Mannings & Sargent (1997); (b) A. Dutrey, personal communication (c) Natta et al. (1999); (d) This paper.

was of high photometric stability, with standard star spectrophotometry consistent within 2%. The best night during the second run, 8 November 1997 UT, had spectrophotometric consistency at a level of about 8%. The spectra for a given run were scaled to the flux level measured on the best night, using the following flux scaling factors: 1.20 for 5 October 1996 UT, 1.05 for 6 October 1996 UT, 1.00 for 11 October 1996 UT, 1.12 for 12 October 1996 UT, 1.00 for 7 November 1997 UT, and 1.30 for 8 November 1997 UT. After scaling, a stastically-weighted average spectrum for each epoch was computed from all the nights, and degraded to $\Delta\lambda \approx 0.1$ μm per detector for October 1996 and to $\approx$0.2 μm per detector for November 1997. The resultant signal-to-noise ratios were 20−30 across the silicate feature, except for the ozone band (O_3 from 9.4−9.8 μm), and 5 or better at the short and long wavelength ends of the atmospheric window. In November 1997, the flux density of the silicate feature and mid-IR continuum (defined shortward of 8.2 μm and longward of 12.5 μm) was multiplied by a factor of 1.11 to match the flux density of October 1996 spectra. The difference in fluxes between the two epochs is slightly larger than the photometric uncertainty.

3. Results

3.1. Millimeter interferometry

The results of millimeter interferometry for the four stars are summarized in Table 2, which gives in Col. 1 the name of the star, in Cols. 2 and 3 the coordinates of the millimeter peak, in Cols. 4–7 the observed wavelengths and fluxes, in Col. 8 the spectral index $\alpha_{\rm mm}$ between the two wavelengths ($F_\nu \propto \lambda^{-\alpha_{\rm mm}}$), in Col. 9 the $FWHM$ size, in Col. 10 the disk mass derived from the observed flux assuming optically thin emission, in Cols. 11 and 12 the interferometer where the observations have been obtained and related references.

All the four stars have millimeter continuum emission which is well detected by the interferometers. This is a strong, albeit indirect, proof that the emitting dust must be distributed in a highly asymmetric manner, i.e., in a circumstellar disk (Beckwith et al. 1990). In the two nearest stars (AB Aur and CQ Tau), the continuum emission is resolved by the interferometers, confirming its disk-like structure (Dutrey et al., private communication). The existence of a disk in AB Aur is proved further by interferometric maps in the CO lines, which resolve the emission and show a velocity pattern typical of rotation (Mannings & Sargent 1997).

The disk mass (gas and dust) in Table 2 has been computed from the 1.3 mm flux assuming that the emission is optically thin:

$$M_{\rm D} = d^2 \frac{F_{1.3\ {\rm mm}}}{\kappa_{1.3\ {\rm mm}} B_{1.3\ {\rm mm}}(T_{\rm D})} \quad (1)$$

where d is the distance of the star, $\kappa_{1.3\ {\rm mm}} = 0.01$ cm^2 g^{-1}, and $T_{\rm D} = 28$ K for the three A stars and 16 K for CQ Tau (Natta et al. 2000a). The four stars have values of $M_{\rm D}$ between 0.02 and 0.05 $M_\odot$, typical of HAe stars. Note that in reality $M_{\rm D}$ depends also on the radial distributions of the disk surface density and temperature (see, for example, Beckwith et al. 1990). Also, the assumption that the millimetric emission is optically thin may not hold. Natta et al. (1999) discuss the possibility that UX Ori, which has a black-body-like millimeter emission ($F_\nu \propto \lambda^{-2}$), has a disk which is optically thick at millimeter wavelengths and estimate the required disk mass to be $\gtrsim$0.1 $M_\odot$.

The spectral index in the millimeter range probed by the interferometers is quite low when compared to the value of $\sim$4 expected for the optically thin emission of small grains, ranging from 2.1 in UX Ori to 3.1 in AB Aur. Note that there are no published interferometer measurements of AB Aur at 1.3 mm, so that the spectral index we computed combining a single-dish and an interferometric observation may be overestimated.

3.2. SEDs

The SEDs of the four stars are shown in Fig. 1. References for the observed fluxes are given in the figure caption. In Table 3, we give for each star the observed excess luminosity after subtraction of the stellar emission ($L_{\rm IR}$), the excess luminosity between 1.25 and 7 μm, i.e., shortward of the silicate feature ($L_{\rm NIR}$), the luminosity in the silicate feature $L_{\rm sil}$, computed by subtracting from the observed

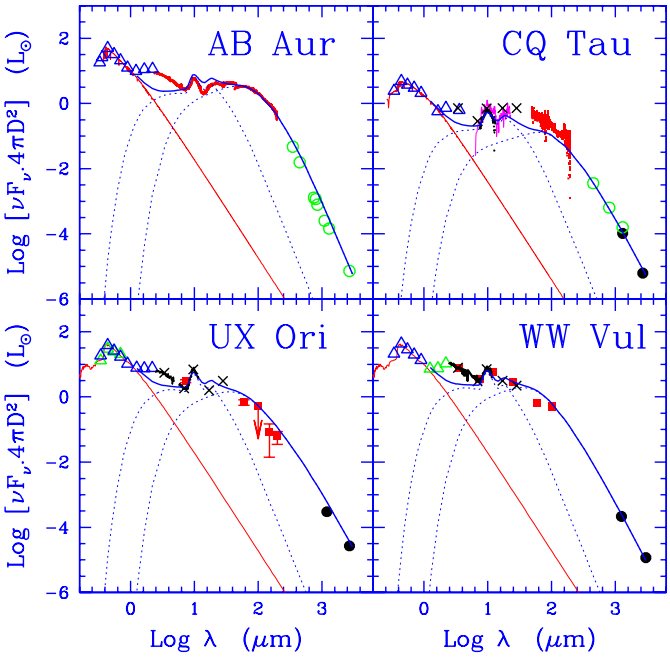

Fig. 1. SEDs of the four stars in the sample. For AB Aur, triangles and open dots plot ground-based fluxes (Mannings 1994 and references therein), while the thick line is the ISO SWS+LWS spectrum (Bouwman et al. 2000). For CQ Tau, visual (Rostopchina, private communication) and near-IR (Glass & Penston 1974) fluxes are shown by triangles, SWS points (Thi et al. 2001) by crosses, the LWS spectrum by small dots at $\lambda > 40$ μm, the open dots are JCMT data from Mannings (unpublished data), the large filled dots from Dutrey et al. (private communication); at 10 μm, both ground-based photometry from this paper (small dots) and LRS-IRAS data are shown. For UX Ori, the symbols are as follows (see Natta et al. 1999 and references therein): visual and near-IR photometry (triangles), ISO-PHOT (squares), PHOT-S (small dots), SWS (crosses), PdB (large filled dots). For WW Vul, visual and near-IR photometry are from Rostopchina (private communication) and Glass & Penston (1974), crosses are SWS points from Thi et al. (2001); PHOT-S (thich line), PHOT (squares) and PdB (filled dots) fluxes from this paper. The observed fluxes have been de-reddened using the values of A_V in Table 1. The thin lines show for each star the adopted photospheric spectrum (Kurucz 1979). Thick solid lines show the predictions of CG97 disk models (Sect. 4); dotted lines the separate contribution of the disk surface and midplane

fluxes a power-law continuum between 7.7 and ∼13 μm, and the ratio of the flux at the peak of the feature to that at 7.7 μm ($F_{\rm peak}/F_{7.7\,\mu{\rm m}}$).

Detailed aspects of the SEDs will be discussed in the following section. Here we want to note that the infrared excess of these stars is a large fraction of the stellar luminosity, varying between 35 and 44%. This is much more than the maximum fraction (25%) expected from a flat reprocessing disk extending from the stellar surface to infinity. It is possible in principle that additional excess luminosity is produced by viscous heating of an accreting disk. However, the "missing" luminosity (∼20% $L_\star$) requires a very high accretion rate (∼10^{-6} $M_\odot$ yr^{-1}), much higher than current estimates in HAeBe stars (Ghandour et al. 1994; Tambovtseva et al. 2001). Accretion, as shown by Hartmann et al. (1993), cannot contribute significantly to the observed SEDs of HAe stars.

Another interesting aspect of the SEDs is the strong 10 μm silicate feature in emission shown by all four stars. The luminosity in the feature is between 2 and 4% of the stellar luminosity and the ratio $F_{\rm peak}/F_{7.7\,\mu{\rm m}}$ varies betwen 2.5 and 4.7. Both quantities are somewhat higher than observed in a sample of 9 T Tauri stars (TTS) in Chameleon by Natta et al. (2000b), who found that in 8/9 stars $F_{\rm peak}/F_{7.7\,\mu{\rm m}}$ ranges from 0.2 to 3.7 and $L_{\rm sil}/L_\star$ from 0.2 to 2%.

Figure 2 shows in detail the shape of the 10 μm silicate feature for the four stars, to which we have added GlassIa, a K4 star in Chamaleon with an unusually strong IR excess, discussed in Natta et al. (2000b). We overlay for comparison the spectrum of AB Aur to that of the other stars (thin lines). For UX Ori, Fig. 2 shows the three spectra, the 1997 ISOPHOT one and the two HIFOGS spectra of 1996 and 1997. The HIFOGS fluxes are about 25% lower than the PHOT-S values, with a peak ratio $F_{\rm peak}/F_{7.7\,\mu{\rm m}} \sim 4.0$ and $L_{\rm sil}/L_\star \sim 0.03$. The normalized profiles are very similar at short wavelength, but differ at long wavelength, especially around 11 μm, where the HIFOGS data indicate a narrower profile. The difference could be due to different beams (18″ for PHOT-S and 3″ for HIFOGS), or to time variabilty. At present, however, given the uncertainty on the absolute calibration, it is difficult to decide if the difference is significant or not.

The shape of the feature shows small variations from star to star, with AB Aur being somewhat narrower on the short wavelength side. The GlassIa silicate feature was fit by Natta et al. (2000b) with mixtures of amorphous pyroxene and olivine with radius 0.1–1 μm. In all of the stars, there is a hint of excess emission around 8.5 μm of uncertain identification. There is no convincing evidence of the 11.3 μm component due to cristalline silicates, seen in some isolated HAe stars (Bouwman et al. 2001). AB Aur shows PAH features at 6.2, 7.6 and 12.3 μm (Bouwman et al. 2000). No features of comparable intensity are seen in the other stars, although we cannot rule out the presence of low-intensity features at other PAH wavelengths (see, for example, the 6.9 μm bump in the spectrum of WW Vul, or the small, but significant variation of the shape of the silicate feature at 8.6 and 11.2 μm between the two HIFOGS spectra of UX Ori).

4. Disk models

We have computed for the four stars the SEDs predicted by disk models, following Chiang & Goldreich (1997; CG97 in the following). In these models, the disk is isothermal in the vertical direction and in hydrostatic equilibrium so that its pressure scale height is a growing function of the distance from the star (flared disk; see Kenyon & Hartmann 1987). The flux at each wavelength is the sum of the emission of the disk midplane and of an

Table 3. Infrared excess

(1)	(2)	(3)	(4)	(5)	(6)	(7)	(8)
Star	$L_{\rm IR}$ ($L_\odot$)	$L_{\rm IR}/L_\star$	$L_{\rm NIR}$ ($L_\odot$)	$L_{\rm NIR}/L_\star$	$L_{\rm sil}$ ($L_\odot$)	$L_{\rm sil}/L_\star$	$F_{\rm peak}/F_{7.7\mu{\rm m}}$
AB Aur	21.3	0.44	11.1	0.23	1.0	0.02	2.5
CQ Tau	1.8	0.36	0.6	0.12	0.16	0.03	4.1
UX Ori	14.6	0.35	7.8	0.18	1.6	0.04	4.7
WW Vul	18.0	0.42	11.0	0.25	1.1	0.03	3.2

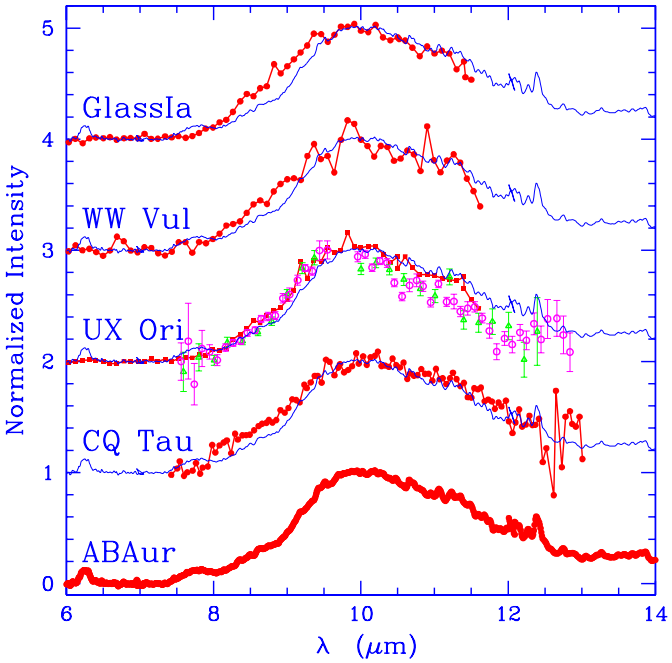

Fig. 2. Profile of the 10 μm silicate feature for the four stars in this paper and Glass Ia. For each star we have subtracted a linear continuum between 7.7 and 13 μm and normalized to the peak intensity (Jy). For each star, the dots are the observed points: SWS data for AB Aur (Bouwman et al. 2000), PHOT-S for WW Vul (this paper) and Glass Ia (Natta et al. 2000b), HIFOGS for CQ Tau (this paper). For UX Ori we show PHOT-S data (Natta et al. 1999; squares) and the two spectra taken with HIFOGS in 1996 (circles) and 1997 (triangles) (this paper). The thin line shows the AB Aur profile, that we repeat on each panel to facilitate the comparison

optically thin, hotter surface layer, often referred to as the disk atmosphere (Calvet et al. 1991), which does not affect the physical structure of the disk, but dominates the SED in the mid-infrared.

The CG97 models need to specify a large number of parameters which are not well constrained by the SED alone (Chiang et al. 2001). However, some of these parameters can be derived from independent observations, namely the stellar properties, the disk inclination θ (Table 1) and the disk outer radius, which we have taken equal to the observed millimeter continuum size. In fact, this is only a lower limit to the physical size (Dutrey et al. 1996), which can be much larger if the disk surface density is a weak function of radius. Of the remaining disk parameters, we

Table 4. Disk parameters

(1)	(2)	(3)	(4)	(5)	(6)
Star	$M_{\rm D}$ ($M_\odot$)	$R_{\rm i}$ (AU)	$R_{\rm D}$ (AU)	p	β
AB Aur	0.01	0.4	100	1.5	2.0
CQ Tau	0.02	0.1	50	1.5	1.0
UX Ori	0.08	0.3	50	1.5	1.0
WW Vul	0.02	0.3	50	1.5	1.0

have fixed the surface density profile to be $\Sigma \propto r^{-p}$ with $p = 1.5$. The disk inner radius $R_{\rm i}$ is defined by the condition $T(R_{\rm i}) = 1500$ K, where T is the temperature of a black body directly exposed to the stellar radiation (see Sect. 4.3 for further discussion of this point). The CG97 models allow us to use different grain properties in the disk midplane and atmosphere. For the midplane, we make the usual assumption $k_{1.3\,{\rm mm}} = 0.01$ cm^2 g^{-1}, $\kappa \propto \lambda^{-\beta}$ and varied β. Since the disks we consider are optically thin only at long wavelengths, the description of the opacity as a power-law function of λ is adequate. The grains in the disk atmosphere are likely to be significantly smaller than those in the disk midplane. We have assumed a mixture of graphite and astronomical silicates (Draine & Lee 1984) with a size distribution as in MRN between 0.01 and 1 μm for both species. About 1/3 of the cosmic abundance of C and all Si is locked into grains. We have followed Chiang et al. (2001) in computing the heating of the disk midplane caused by a mixture of grains in the atmosphere.

The adopted parameters are summarized in Table 4. Note that the disk masses derived from the fits are within a factor ∼2 of those computed using Eq. (1) and given in Table 2. The model-predicted SEDs are shown in Fig. 1; the solid lines show the total emission and the thin dotted lines the separate contribution of the disk midplane and atmosphere.

4.1. The long-wavelength part of the SEDs

The disk models provide a rather good fit to the long-wavelength part of the SEDs. The choice $p = 1.5$, $\beta = 1$ works well for three of our four stars, the only exception being AB Aur, which has an extremely steep spectrum at long wavelengths and requires $\beta \sim 2$. This suggests that the grains in the AB Aur disk midplane are smaller than those in the three UXORs. The possibility of grain

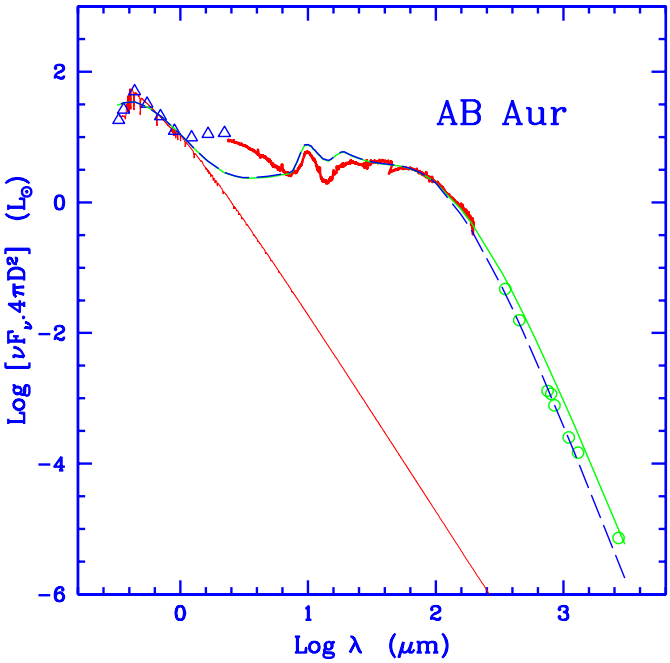

Fig. 3. Disk models for AB Aur with different surface density profiles. The solid line is for $p = 1.5$, $M_{\rm D} = 0.01\ M_\odot$ (same as Fig. 1), the dashed line for $p = 15/14$, $M_{\rm D} = 0.007\ M_\odot$. All the other parameters are as in Fig. 1

evolution (i.e., coagulation) among HAe stars is suggested by Meeus et al. (2001). These authors find that the submillimeter spectral index in a sample of 12 stars decreases from values $\gtrsim$3 in AB Aur and HD 179218 (which according to its location on the HR diagram is only 10^5 yr old), to values of $\sim$2 in a number of isolated HAe stars. It is tempting to associate "large grains" to UXORs and interpret their variability as a result of aging disks. However, this may be premature, since there are a number of counterexamples. Just to quote one, HD 163296 has spectral index $\sim$2 and no evidence of large variability (Herbst & Shevchenko 1998). This issue needs to be addressed again with the help of observations at longer wavelengths (several HAe stars with flat spectral index may be detected at 7 mm with the VLA) and spatially resolved continuum maps.

In the far-infrared, there is room for improvements, especially in the case of CQ Tau, where the model predicted flux is lower than observed by a factor $\sim$2–3 in the interval $\sim$30–150 μm. Chiang et al. (2001) have recently presented an improved version of the CG97 disk models, where a more realistic dust model is adopted. They show that ices are important contributors to the outer disk opacity, and that taking into account intermolecular translational modes of water ice at 45, 62 and 154 μm improves the fit to the CQ Tau SED. However, the dependence of the disk midplane emission on θ may also play a role, since at the very high inclination of CQ Tau a small change in θ may change significantly the predicted emission of the optically thick disk midplane.

In spite of the rather good fit, it is important to remember that the law $\Sigma \propto R^{-1.5}$ is an ad hoc law derived by Hayashi (1981) for the Solar system. In a steady accretion disk, it is $\Sigma = \dot{M}/(\alpha c_{\rm s} h)$, where $\dot{M}$ is the accretion rate through the disk and one makes the usual assumption that the viscosity is proportional to the sound speed $c_{\rm s}$ and pressure scale height h via the coefficient α. Using for $c_{\rm s}$ and h the radial dependence derived by CG97 (for optically thick disks), one obtains $p = 15/14$, assuming that α does not depend on R. More realistic disk models predict more complex surface density profiles, generally flatter than a $p = 1.5$ power-law (D'Alessio et al. 1998; Papaloizou & Terquem 1999). Models with $p = 15/14$ fit the data well, as shown for the case of AB Aur in Fig. 3. The $p = 15/14$ disk is slightly less massive ($M_{\rm d} = 0.007\ M_\odot$) than the $p = 1.5$ disk and has lower surface density in its inner parts.

4.2. Mid-infrared and silicate emission

In the mid-infrared, the SED is dominated by the emission of the disk atmosphere. The models of Fig. 1 reproduce the observations reasonably well. In general, disk models which include the optically thin disk atmosphere can reproduce the intensity of the observed dust emission features and mid-infrared emission (see also Chiang et al. 2001). They can also account for the observed variations from star to star and among stars of similar properties in terms of relatively small changes of the characteristics of grains in the disk atmospheres. In the CG97 models, the emission at each wavelength λ is proportional to the ratio $\kappa_\lambda/\kappa_\star$, where $\kappa_\star$ is the opacity at the frequency where the stellar radiation peaks, i.e., about 0.3–0.4 μm for the HAe stars. In many dust models, the mid-infrared opacity is dominated by silicates, while $\kappa_\star$ is due to carbonaceous grains (graphite in our case). One can vary the intensity of the mid-infrared emission by changing $\kappa_\star$, either by varying the fraction of carbon in grains or the size distribution of graphite. Figure 4 shows, for example, the intensity of the 10 μm feature when the amount of cosmic carbon locked into graphite varies from 100% (long-dashed line) to 3% (solid line). The relative intensity of the feature $F_{\rm peak}/F_{7.7\,\mu{\rm m}}$ increases from about 2 to 5.4. Our assumption that 30% of cosmic carbon is in graphite gives $F_{\rm peak}/F_{7.7\,\mu{\rm m}} \sim 3.2$. One could reproduce the range of observed values of $F_{\rm peak}/F_{7.7\,\mu{\rm m}}$ by varying the fraction of carbon in grains between 10% and 50%. Alternatively, if the maximum size of graphite grains is 0.12 μm, rather than 1 μm, $\kappa_{10\mu{\rm m}}/\kappa_\star$ decreases from 0.52 to 0.32, and $F_{\rm peak}/F_{7.7\,\mu{\rm m}}$decreases from 3.2 to 2.0. Changes in $F_{\rm peak}/F_{7.7\,\mu{\rm m}}$ can also be due to variations in the composition and size distribution of the silicates themselves. The low value of $F_{\rm peak}/F_{7.7\,\mu{\rm m}}$ and of the overall mid-infrared emission in AB Aur can be understood if the grains in the disk atmosphere (as well as those in the midplane) are somewhat smaller than in the other stars. Note that graphite can be replaced wholly or in part by other

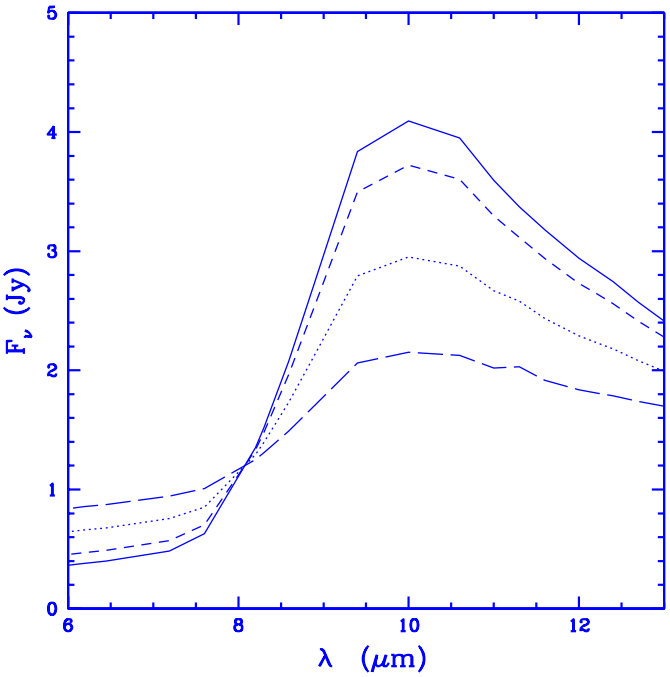

Fig. 4. Model-predicted silicate feature for UX Ori for increasing fraction of carbon locked in graphite grains, from 3% (solid line) to 10% (short-dashed line), 30% (dotted line) and 100% (long-dashed line). All other parameters as in Fig. 1

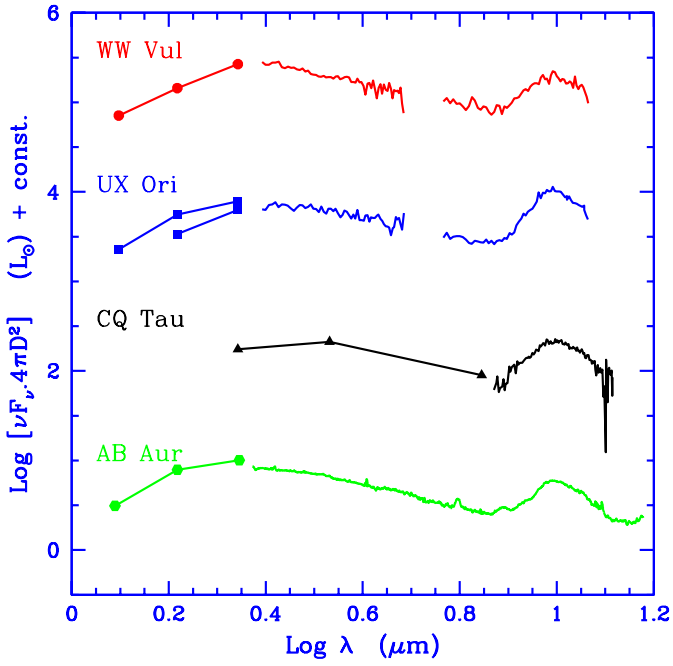

Fig. 5. Observed near and mid-IR spectra of the four stars, as labelled, after subtraction of the photospheric emission

grain species, such as metallic Fe, whithout changing our results. Variations in the grain size and in the proportion of the various materials from star to star are seen in the ISO spectra of HAe stars (Bouwman et al. 2001).

The cross section of "astronomical" silicates we have used is a more accurate description of the silicates in the diffuse ISM than in pre-main–sequence circumstellar disks, where a mixture of largish pyroxene and olivine grains provides a better fit to the shape of the 10 and 20 μm features (Reimann et al. 1997; Natta et al. 1999, 2000b; Bouwman et al. 2001). However, a study of the mineralogy of grains in the disk is not the scope of this paper. We just want to point out that CG97 models can be used to investigate the mineralogy of dust, and, in particular, the nature of the silicates present at the disk atmosphere.

4.3. The near-infrared excess

The only serious failure of the CG disk models is their inability to account for the large excess luminosity in the near-infrared seen in all the stars. This old problem (Hartmann et al. 1993) has been recently rediscussed by Natta et al. (1999) in their study of UX Ori and noted by Chiang et al. (2001) in all the HAe stars in their sample. No satisfactory solution has so far been proposed. We will discuss it here again in more detail, and propose a modification of the structure of the inner disk which may explain the observations.

We focus in this section on the emission in the range of wavelengths 1.25–7 μm, (which we will call "near infrared" in the following) which is shown in detail in Fig. 5. For each star we have subtracted from the observed emission the stellar contribution, as shown in Fig. 1. This is a large fraction of the total in the near-infrared, about 70% in J, 30–50% in H, 10–20% in K for the three A stars. For CQ Tau, the star contributes 100% of the H flux, and is still 45% of the total in K. As a consequence, the disk fluxes at shorter wavelengths are very uncertain, since they are strongly affected by uncertainties on the stellar parameters and extinction and by the variability of the star in the visual and near-infrared. This is shown, for example, by the two sets of points for UX Ori, which correspond to two observations at different epochs.

In spite of these caveats, there are a number of characteristics worth noticing. First of all, the four stars have very similar SEDs, with a peak in νF_ν around 2 μm and a sharp decrease at shorter wavelengths (the $\sim$3 μm bump; Hillenbrand et al. 1995; Hartmann et al. 1993). Between $\sim$3 and 7 μm the SEDs have an almost identical shape. The dependence of νF_ν on wavelength is flat, roughly as $\lambda^{-(1.1-1.3)}$. This is typical of the SED of geometrically flat, optically thick disks, where $F_\nu \propto \lambda^{-4/3}$.

The excess luminosity in the near-infrared is rather large, ranging between 12 and 25% of the stellar luminosity (see Table 3). These values are comparable to the fraction of stellar light intercepted and re-radiated in the near-infrared by the inner regions of a flat disk. However, the conclusion that flat disks can account for the observed near-infrared properties of HAe stars is very likely incorrect.

A flat disk intercepts a maximum 25% of the stellar radiation only if it extends inward all the way to the stellar radius. This cannot be the case in HAe stars, as

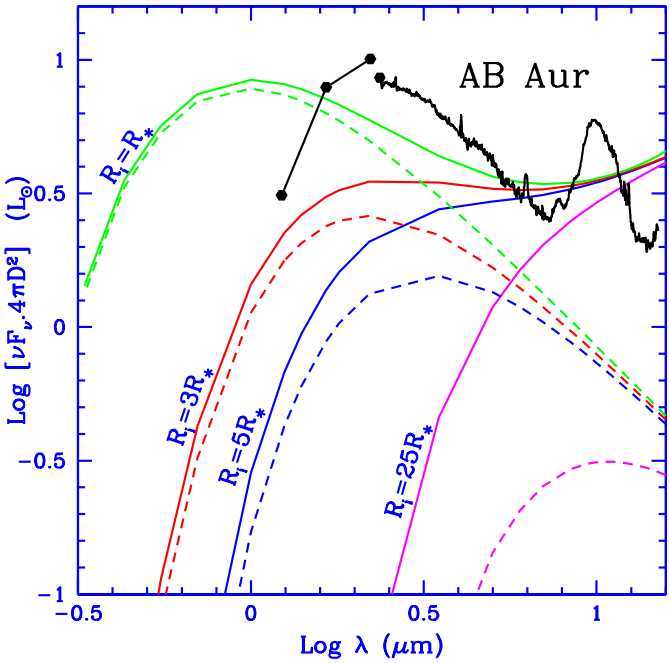

Fig. 6. Disk model predictions for AB Aur. Dashed lines are for flat disks, solid lines for flared ones. The inner radius R_i increases from $R_\star$ to 25 $R_\star$, as labelled. All other parameters are the same. The dots and the thick solid line show the observed spectrum, after subtraction of the photospheric component (same as Fig. 5)

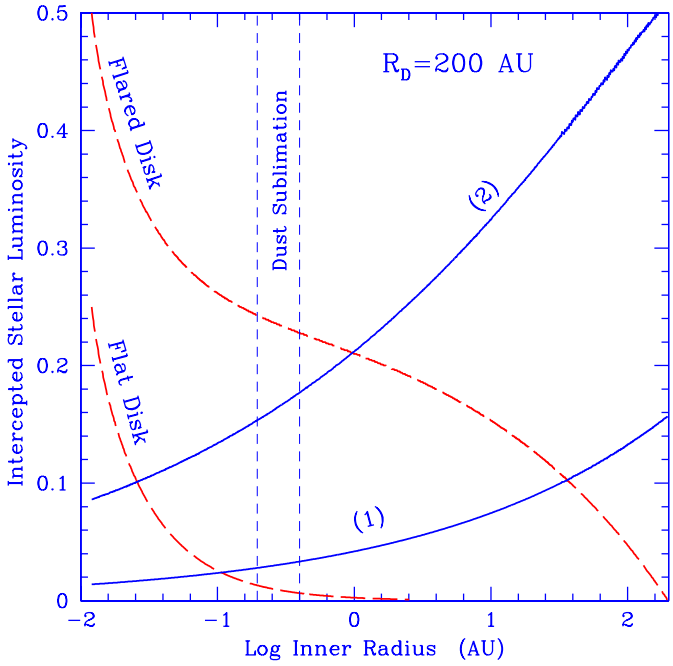

Fig. 7. Fraction of the stellar luminosity intercepted by disks with outer radius R_D = 200 AU and increasing inner radius R_i. Both flat and flared disks are plotted (dashed curves). The solid lines show the fraction of stellar light intercepted by the inner disk wall at R_i computed as H_i/R_i, i.e., assuming that the wall has the shape of a cylinder of height H_i. In curve (1) H_i is equal to the pressure scale height h, in curve (2) to the height of the disk photosphere. The vertical thin dashed lines show the location of T = 1500 and 2000 K. The stellar parameters are those of AB Aur

illustrated in Fig. 6. Flat disks that extend to the stellar radius reproduce the observed value of L_{NIR}, but their emission peaks at wavelengths which are too short, typically 0.8 rather than 2 μm. In the range 3–7 μm, even a model with $R_i = R_\star$ predicts values of νF_ν a factor of 2 lower than observed. Disks with large inner holes have a SED that peaks at longer wavelengths, but the fraction of stellar light intercepted and re-emitted is far too small.

Figure 7 shows the fraction of stellar radiation intercepted by flat and flared disks of increasing inner radius. Flat disks with $R_i = R_\star$(∼0.01 AU) intercept 25% of the stellar radiation (independently on stellar and disk parameters as long as $R_D \gg R_\star$), while flared disks intercept significantly more. The exact value depends on the disk flaring and outer radius; it is about 50% in the case shown in the figure. If R_i increases, the fraction of intercepted stellar light decreases rapidly. For $R_i \sim 0.3$ AU (∼25 $R_\star$), it is almost zero in the case of flat disks and of the order of 25% for flared disks. This is also significantly less than observed; it increases to 40% only for R_D = 1000 AU. Moreover, as shown in Fig. 6, the emission of flared disks with large R_i is always peaked at longer wavelengths, not in the near-IR. We find no way in which either flat or flared disk models can account for the observed SEDs over the whole range of wavelengths.

The models discussed so far consider only the fraction of stellar radiation intercepted by the disk surface. In fact, if the disk has a large inner radius, there is an additional region, roughly shaped as a cylinder of radius R_i and height H_i, which also intercepts and re-radiates a fraction of the stellar light. This inner *wall* is much hotter and has therefore a much bigger scale height than a CG disk at the same distance from the star, because it sees the stellar surface almost perpendicularly. The exact amount of intercepted radiation may be significant. As a zero order indication, we show in Fig. 7 the values for a wall at R_i with $H_i = h$, where h is the scale height of the disk at the temperature of the wall (curve 1) and $H_i = H$, where H is the photospheric height (∼4−5h; curve 2).

The vertical dashed lines in Fig. 7 show the approximate region where we expect dust evaporation to occur. Thus, if the inner radius of the disk is determined by dust evaporation, then $R_i \sim 0.3$ AU, and the fraction of stellar radiation intercepted by the inner wall can be as high as 20%, while the disk surface will intercept about 25% of the stellar radiation. These numbers are roughly consistent with the values observed in AB Aur and in the other HAe stars in our sample. We show for example in Fig. 8 the AB Aur SED where we have added to the disk emission shown in Fig. 1, a BB component at T = 1700 K corresponding to an inner wall at $R \sim 0.27$ AU which intercepts about 30% of the stellar radiation. While the fit to the data is not perfect, it is clear that the model we propose decreases the discrepancy between models and observations. However, more detailed models are in order,

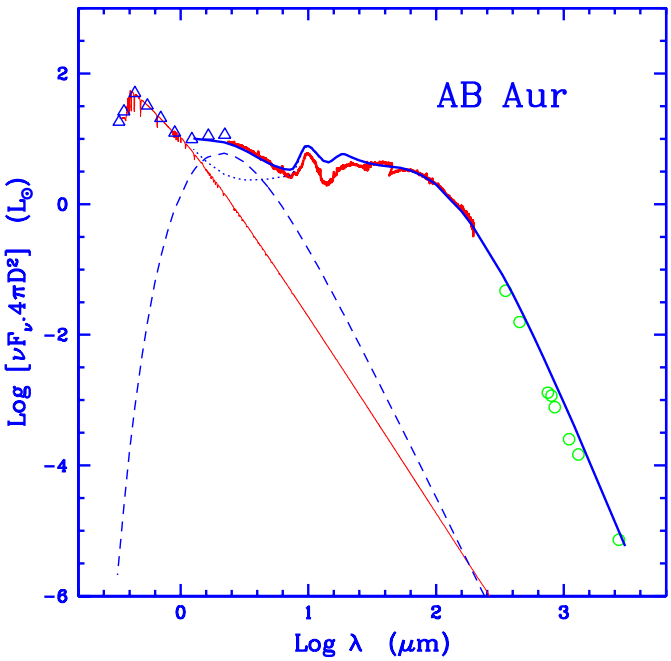

Fig. 8. Model-predicted SED of AB Aur, same as Fig. 1 (dotted line). We have added the emission of the inner disk wall, as described in the text (dashed line). The total is shown by the solid line

which include, among others, the effect of the shade that the puffed-up inner wall projects over the disk at larger radii (Dullemond et al. 2001).

This scenario, of a flared disk with a large inner hole determined by dust evaporation, appears consistent with the recent results of near-IR interferometry of Millan-Gabet et al. (2001). They find that the visibility data in J, H, K for AB Aur are best fit by a model where the emission is coming from a ring of radius ∼0.3 AU, seen almost face-on. In our scenario, the Millan-Gabet et al. ring is just the inner wall of the disk, which dominates the observed near-infrared emission.

5. Discussion and conclusions

We have presented in this paper state-of-the-art SEDs of four HAe stars, and discussed them in the context of circumstellar disk models. We have used the simplified description of the disk structure and emission outlined by Chiang & Goldreich (1997). The disk is in hydrostatic equilibrium in the vertical direction at the temperature of the disk midplane (flared disk). Its emission is computed as the sum of the emission of the optically thick midplane and of the optically thin, overheated surface layers. The properties of grains in the midplane and atmosphere can be independently specified.

These models provide a good fit to the observations, if the disk is truncated at an inner radius of a few tenths of AU. This roughly corresponds to typical dust sublimation temperatures (1500–2000 K), if we consider that the inner "wall" of the flared disk is exposed directly to the stellar radiation, and is therefore much hotter than the disk midplane, which receives the stellar radiation at a small grazing angle. The inner wall is then puffed-up with respect to the disk, and intercepts a significant fraction of the stellar radiation, which increases with the inner radius $R_{\rm i}$. The emission of the inner wall is mostly in the near-infrared and can in principle account for the observed shape and luminosity at these wavelengths, which has been a long-standing puzzle. We suggest that the recent interferometric observations of AB Aur obtained by Millan-Gabet et al. (2001) in H and K detect exactly the emission of this wall, which at these wavelengths looks like a ring on the plane of the sky.

One of the implications of the above disk model is that there is no significant absorption between the star and the inner wall. In other words, any gas within $R_{\rm i}$ must be optically thin to the stellar radiation. This is not the case for the disk models considered in Sect. 4, where we have adopted a surface density profile $\Sigma \propto R^{-1.5}$ and derived the disk mass required to fit the long-wavelength fluxes. With the usual assumption of a gas-to-dust mass ratio of 100, the optical depth of the inner *gaseous* disk is very large (about 500–1000 at $R_{\rm i}$, assuming that the opacity is mostly due to H^-; see Hartmann et al. 1993). The gas absorbs efficiently the stellar radiation, so that dust sublimation occurs much closer to the star (at about 2–3 $R_\star$), where the disk midplane temperature, which is significantly lower that that of the unscreened wall, reaches dust sublimation values. However, the surface density of the inner disk is not constrained by the data, as long as the disk remains optically thick at $R > R_{\rm i}$. The CG97 model with $\Sigma \propto R^{-15/14}$ (Fig. 3) has surface density at $R_{\rm i}$ 40 times lower than our standard model, and an optical depth to the stellar radiation of only about 10–20. This model corresponds to an accretion rate $\dot{M} \sim 10^{-8}\ M_\odot$ (for a viscosity coefficient $\alpha = 0.01$), in agreement with the low accretion rates expected in HAe stars (Hartmann et al. 1993; Ghandour et al. 1994). It is possible that the amount of gas in the inner disk is even lower (if, for example, the viscosity coefficient α is not constant). Before speculating further, however, the effect of the sudden increase of the opacity due to dust sublimation (by more than a factor 1000) in disks where the gas opacity is not extremely large, as well as the stability of the resulting geometry, should be addressed in detail.

As far as the emission at longer wavelengths is concerned, we confirm previous results that CG97 disk models can account for the observed SEDs not only of TTS but also of HAe stars. The mid-IR, as well as the emission in any dust feature, is dominated by the emission of the optically thin surface layers. Although we have not addressed the dust mineralogy in any detail, we find that energetically CG models can account for the observations. The dust in the disk atmosphere is probably a mixture of largish silicates and carbonaceous materials. At even longer wavelengths, dust in the disk midplane dominates the emission; however, the degeneracy of the SED with respect to dust and disk parameters does not allow more

than a check of consistency between models and observations.

In summary, most of the known properties of Herbig Ae stars can be well explained by models where the circumstellar matter is confined to a disk. We suggest here that a proper treatement of the structure of the inner disk may solve the long-standing puzzle of the near-infrared properties of these stars. Namely, we notice that for low accretion rates the inner gaseous disk is optically thin, the optically thick dust wall produced by dust condensation is exposed directly to the stellar radiation and is therefore puffed-up with respect to the cooler disk midplane. The SED is the result of the emission of three different parts of the disk, namely the inner wall in the near-infrared, the optically thin atmosphere in the mid-infrared, the midplane at sub-millimeter and millimeter wavelengths.

Disks in TTS must be very similar. The lack of the "3 μm" bump in stars of later spectral type can be easily understood if we consider that the effects of the inner wall become less and less relevant as the stellar luminosity decreases and $R_{\rm i}$ approaches $R_\star$. Moreover, if, as we suspect, the accretion rates of the classical TTS are on average higher than in HAe stars, the inner gas disk is more optically thick, with the effect of decreasing $R_{\rm i}$ even further. The dependence of the wall emission on the spectral type of the central star is currently under investigation (Dullemond et al. 2001).

Of the goals stated in Sect. 1, two concerned more specifically the nature of UXORs. There is no significant difference in the inferred disk structure between the three UXORs and AB Aur, with the single exception that grains in AB Aur are probably smaller than in the other three stars. The significance of this last point, however, is not clear, since the degree of variability of AB Aur is dubious. It needs to be confirmed in a larger sample of photometrically stable HAe stars before we can interpret it as a hint of an evolutionary difference between the two groups.

We do not find any clue to the nature of the dust enhancements that occasionally occult the three UXORs. However, we note that the inner wall is potentially a promising location for the "clumps". At $R_{\rm i}$, the sound speed is a few km s^{-1} so that density enhancements of stellar size can grow and dissipate on timescales of a few days, which are typical of UXOR minima. The fact that we expect that such walls will be less relevant in cooler stars may explain the relative lower fraction of UXORs among TTS. However, in order for the line of sight to intercept the wall, one needs to see the disk at large inclination, larger than about 75 deg in our examples. This is much more edge-on than found by Natta & Whitney (2000) from the polarization of the visual light during photospheric minima. For such values of the inclination we expect that the outer disk will obscure the star at all times (Bertout 2000). In spite of these difficulties, we feel that the role of density fluctuations near the dust sublimation radius should be investigated further.

Acknowledgements. The discussion of the disk structure in HAe stars has involved many of our collegues, without whom this paper would have not been possible. Among them, I (AN) want to thank in particular Jeroen Bouwman, Carsten Dominik, Kees Dullemond, Alex de Koter and Rens Waters, who have made my visit in Amsterdam most pleasant and fruitful. Very interesting conversations with Nuria Calvet, Claude Bertout and Caroline Terquem have helped in clarifying a number of issues addressed in this paper. We gratefully aknowledge the support of ASI (grants ARS-99-15 and 1/R/27/00) to the Osservatorio Astrofisico di Arcetri. This research has made use of the SIMBAD database, operated at CDS, Strasbourg, France.

References

Ashok, N. M., Chandrasekhar, T., Bhatt, H. C., & Manoj, P. 1999, IAU Circ., 7103, 1
Beckwith, S. V. W., Sargent, A. I., Chini, R. S., & Güsten, R. 1990, AJ, 99, 924
Bertout, C. 2000, A&A, 363, 984
Bouwman, J., de Koter, A., van den Ancker, M. E., & Waters, L. B. F. M. 2000, A&A, 360, 213
Bouwman, J., Meeus, G., de Koter, A., et al. 2001, A&A, submitted
Calvet, N., Patino, A., Magris, G. C., & D'alessio, P. 1991, ApJ, 380, 617
Chiang, E. I., & Goldreich, P. 1997, ApJ, 490, 368
Chiang, E. I., Joung, M. K., Creech-Eakman, M. J., et al. 2001, ApJ, 547, 1077
Cohen, M., Witteborn, F. C., Carbon, D. F., et al. 1996, AJ, 112, 2274
D'Alessio, P., Cantó, J., Calvet, N., & Lizano, S. 1998, ApJ, 500, 411
Di Francesco, J., Evans, N. J. II, Harvey, P. M., Mundy, L. G., & Butner, H. M. 1994, ApJ, 432, 710
Draine, B. T., & Lee, H. M. 1984, ApJ, 285, 89
Dullemond, C. P., Dominik, C., & Natta, A. 2001, ApJ, submitted
Dutrey, A., Guilloteau, S., Duvert, G., et al. 1996, A&A, 309, 493
Gabriel, C., Acosta-Pulido, J., Heinrichsen, I., Morris, H., & Tai, W.-M. 1997, PASPC, 125, 108
Ghandour, L., Strom, S., Edwards, S., & Hillenbrand, L. 1994, in ASP Conf. Ser., 62, The Nature and Evolutionary Status of Herbig Ae/Be Stars, ed. P. S. Thé, M. R. Pérez, & E. P. J. van den Heuvel (San Francisco: ASP), 223
Glass, I. S., & Penston, M. V. 1974, MNRAS, 167, 237
Grady, C. A., Woodgate, B., Bruhweiler, F. C., et al. 1999, ApJ, 523, L151
Grady, C. A., Devine, D., Woodgate, B., et al. 2000, ApJ, 544, 895
Grinin, V. P. 1994, in ASP Conf. Ser., 62, The Nature and Evolutionary Status of Herbig Ae/Be Stars, ed. P. S. Thé, M. R. Pérez, & E. P. J. van den Heuvel (San Francisco: ASP), 63
Hartmann, L., Kenyon, S. J., & Calvet, N. 1993, ApJ, 407, 219
Hayashi, C. 1981, PThPS, 70, 35
Herbst, W., & Shevchenko, V. S. 1999, AJ, 118, 1043
Hillenbrand, L. A., Strom, S. E., Vrba, F. J., & Keene, J. 1992, ApJ, 397, 613
Il'in, V. B., & Krivova, N. A. 2000, AstL, 26, 379
Kawabata, T., Kogure, T., Fuji, M., Anyani, K., & Suzuki, M. 1998, IBVS, 4651, 1

Kenyon, S., & Hartmann, L. 1987, ApJ, 323, 714
Kurucz, R. L. 1979, ApJS, 40, 1
Lord, S. D. 1993, NASA Technical Report TM–103957 (Moffet Field: NASA/Ames Research Center)
Mannings, V. 1994, MNRAS, 271, 587
Mannings, V., & Sargent, A. I. 1997, ApJ, 490, 792
Mannings, V., & Sargent, A. I. 2000, ApJ, 529, 391
Meeus, G., Waters, L. B. F. M., Bouwman, J., et al. 2001, A&A, 365, 476
Millan-Gabet, R., Shloerb, F. P., & Traub, W. A. 2001, ApJ, 546, 358
Miroshnichenko, A., Ivezić, Z., & Elitzur, M. 1997, ApJ, 475, L41
Miroshnichenko, A., Ivezić, Z., Vinkovic, D., & Elitzur, M. 1999, ApJ, 520, L11
Natta, A., Grinin, V. P., & Mannings, V. 2000a, in Protostars and Planets IV, ed. V. Mannings, A. P. Boss, & S. S. Russell (Tucson: Univ. of Arizona Press), 559
Natta, A., Grinin, V. P., Mannings, V., & Ungerechts, H. 1997, ApJ, 491, 890
Natta, A., & Krügel, E. 1995, A&A, 302, 849
Natta, A., Meyer, M. R., & Beckwith, S. V. W. 2000b, ApJ, 534, 838
Natta, A., Palla, F., Butner, H. M., Evans, N. J. II, & Harvey, P. M. 1993, ApJ, 406, 674
Natta, A., Prusti, T., Neri, R., et al. 1999, A&A, 350, 541
Natta, A., & Whitney, B. A. 2000, A&A, 364, 633
Papaloizou, J. C. B., & Terquem, C. 1999, ApJ, 521, 823
Pezzuto, S., Strafella, F., & Lorenzetti, D. 1994, ApJ, 485, 290
Reimann, H.-G., Gürtler, J., Friedemann, C., & Käufl, H. U. 1997, A&A, 326, 271
Rostopchina, A. N. 1999, ARep, 43, 113
Tambovtseva, L. V., Grinin, V. P., Rodgers, B., & Kozlova, O. V. 2001, Astron. Rep., in press
Thi, W. F., van Dishoeck, E. F., Blake, G. A., et al. 2001, ApJ, in press
van den Ancker, M. 1999, Ph.D. Thesis, University of Amsterdam
van den Ancker, M., de Winter, D., & Tjin A Djie, H. R. E. 1999a, A&A, 330, 145
van den Ancker, M., Volp, A. W., Pérez, M. R., & de Winter, D. 1999b, IBVS, 4704, 1
Waters, L. B. F. M., & Waelkens, C. 1998, ARA&A, 1998, 36, 233
Witteborn, F. C., Cohen, M., Bregman, J. D., et al. 1995, in Airborne Astronomy Symposium on the Galactic Ecosystem: From Gas to Stars to Dust, ed. M. R. Haas, J. A. Davidson, & E. F. Erickson, ASP Conf. Ser., 73, 573